

## Modeling of Rock Friction

### 2. Simulation of Preseismic Slip

JAMES H. DIETERICH

*U.S. Geological Survey, Menlo Park, California 94025*

The constitutive relations developed in the companion paper are used to model detailed observations of preseismic slip and the onset of unstable slip in biaxial laboratory experiments. The simulations employ a deterministic plane strain finite element model to represent the interactions both within the sliding blocks and between the blocks and the loading apparatus. Both experiments and simulations show that preseismic slip is controlled by initial inhomogeneity of shear stress along the sliding surface relative to the frictional strength. As a consequence of the inhomogeneity, stable slip begins at a point on the surface and the area of slip slowly expands as the external loading increases. A previously proposed correlation between accelerating rates of stable slip and growth of the area of slip is supported by the simulations. In the simulations and in the experiments, unstable slip occurs shortly after a propagating slip event traverses the sliding surface and breaks out at the ends of the sample. In the model the breakout of stable slip causes a sudden acceleration of slip rates. Because of velocity dependency of the constitutive relationship for friction, the rapid acceleration of slip causes a decrease in frictional strength. Instability occurs when the frictional strength decreases with displacement at a rate that exceeds the intrinsic unloading characteristics of the sample and test machine. A simple slider-spring model that does not consider preseismic slip appears to approximate the transition adequately from stable sliding to unstable slip as a function of normal stress, machine stiffness, and surface roughness for small samples. However, for large samples and for natural faults the simulations suggest that the simple model may be inaccurate because it does not take into account potentially large preseismic displacements that will alter the friction parameters prior to instability.

#### INTRODUCTION

The companion paper [Dieterich, 1979] first presents experimental results for friction as a function of time, displacement, and velocity and then develops constitutive relationships that permit a fairly accurate simulation of the experimental phenomena. This portion of the study applies those results to the two-dimensional, plane strain modeling of preseismic slip and the initiation of unstable slip. The motivation for this analysis is twofold. First, some recent experiments [Dieterich, 1978a; Dieterich *et al.*, 1978] provide detailed data for preseismic slip that afford an opportunity to test further the constitutive equations in a system with fairly complicated mechanical interactions. The model presented below has the mechanical elements needed to represent the principal interactions that have been identified in the laboratory experiments. Simulation of earthquake faulting probably involves analogous interactions. The model is two-dimensional, physical properties and stresses along the sliding surface are permitted to vary as a function of position, and the elastic properties of the sample and test apparatus are represented. Second, the process of preseismic slip in laboratory experiments holds obvious interest as a possible earthquake precursor. At present, the applicability of experimental preseismic slip data for earthquake precursor models is quite conjectural because the mechanisms and parameters controlling preseismic slip are poorly understood. The simulations presented here may provide some insight into the mechanics of preseismic slip in laboratory experiments.

#### PRESEISMIC SLIP

Stable slip as a premonitor of unstable (seismic) slip occurs for a variety of experimental conditions and for different types of sliding surfaces [e.g., Scholz *et al.*, 1972; Logan *et al.*, 1972;

Byerlee and Summers, 1975]. While the magnitude of the preseismic slip displacements observed for the studies cited above is extremely variable, it appears that at least small amounts of stable slip always precede slip instability.

Scholz *et al.* [1972] have examined preseismic slip on ground surfaces of Westerly granite under biaxial loading conditions. They observe preseismic displacements of the order of  $10^{-3}$  cm, independent of strain rate. The duration of preseismic slip is inversely proportional to strain rate. Plots of fault displacement against time show accelerating displacement rates up to the time of unstable slip.

The study by Dieterich [1978a] employed a biaxial configuration with Westerly granite (Figure 1) similar to that of Scholz *et al.* [1972]. The principal refinement was the addition of several strain gages adjacent to the surface that permit the propagation of preseismic slip along the surface to be monitored as well as provide detailed measurement of stress and friction variations along the surface. Three gages record strains normal to the slip surface, and thirteen gages record shear strains parallel to the surface.

Two distinct stages of preseismic slip were consistently observed in those experiments. The first stage consists of a slip event that begins at some point on the surface and slowly propagates over most or all of the sliding surface. Figure 2 is a representative example given by Dieterich [1978a]. Shear strains are plotted as a function of time for several locations adjacent to the surface. The curves are arranged by position on the sliding surface, and the numbers labeling the curves correspond to the strain gages shown in Figure 1. Gages 4–16 are the shear bridges with the numbering proceeding from upper right to lower left of the block. Prior to slip, the rams that load the sample increase the shear stress at an approximately constant rate. A leveling or a decrease in strain amplitude indicates slip on the fault adjacent to the strain gage. For the example in Figure 2, slip begins at gage 15 and propagates across the sample. Once slip starts at a location on the fault, stable slip continues at that point until the time of the instability.

This paper is not subject to U.S. copyright. Published in 1979 by the American Geophysical Union.

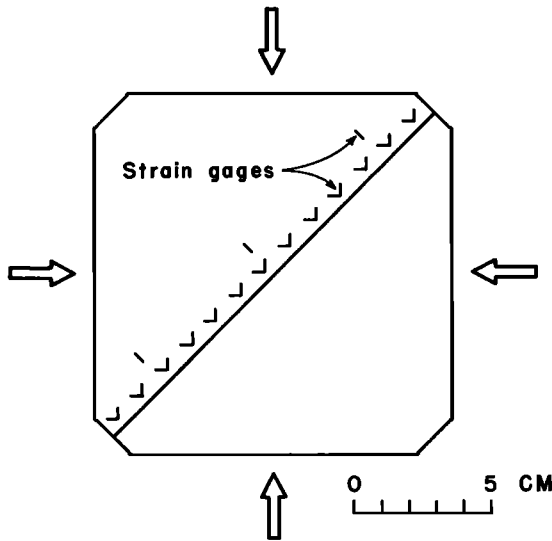


Fig. 1. Schematic diagram of the experiment by Dieterich [1978a]. Arrows indicate loading directions.

The breakout of the first stage of slip at the end of the sliding surface initiates the second stage of slip, which is of very short duration, 0.01–0.001 s. Note in Figure 2 that unstable slip occurs a short time after the slip event reaches the end of the sample at gage 5. While the first stage of slip appears to be intrinsically stable, the second stage rapidly becomes unstable and is characterized by acceleration of slip rates and falling stresses. Other preseismic slip events vary in detail and sometimes show greater complexity than the example in Figure 2. However, all have the common characteristic that unstable slip follows a short interval of falling stresses that is triggered after stage I reaches the end of the sample. Hence most or all of the surface is slowly sliding at approximately constant or slightly decreasing stress at the time that the second stage of slip begins.

Figure 2 gives evidence for velocity-dependent friction because the stresses are higher during the low-velocity stage I slip than during the high-velocity slip of the instability. The companion paper explains that type of velocity dependence as originating from a decrease in the time of asperity contact with increasing velocity. Independent observations show that friction increases with time of contact and hence decreasing velocity of slip. Slip instability in Figure 2 appears to be triggered as a velocity perturbation when the slip event breaks out at the end of the surface. Apparently, a jump in slip velocity occurs that in turn causes the friction to drop suddenly.

The inhomogeneity of stress relative to the critical stress for slip initiation controls the amount of stage I slip. The greater the inhomogeneity, the greater the amount and duration of preseismic slip. For two experiments arranged to give homogeneous stress with respect to the frictional strength, no stage I preseismic slip was evident from the strain records. This suggests a reason for the stability of stage I slip: during the first stage of slip, increasing external load is required to drive the boundary between the slipping and unslipped portions of the surface into the regions where the applied stress is less than the frictional strength [Dieterich, 1978a].

Similar results were obtained in a very large scale biaxial experiment with a sliding surface 200 cm long [Dieterich *et al.*, 1978]. Again, a slowly propagating slip event traversed the surface prior to unstable slip. Comparison of the premonitory displacements from the large- and small-scale experiments in-

dicates that the premonitory displacements scale with fault dimensions.

#### MODEL

Figure 3 illustrates the finite element model used to simulate the experimental configuration of Figure 1. Slip between the two triangular blocks is represented in this model by the motion of a single triangular block on a planar surface. During slip, friction at points along the surface satisfies the relationship developed in the companion paper [Dieterich, 1979]:

$$\mu = [c_1 + c_2 \log(c_3 t + 1)] \left\{ f_1 + \frac{1}{f_2 \log[(f_3/\delta) + 10]} \right\} \quad (1)$$

where  $\mu$  is the coefficient of friction, which is given by the ratio of shear stress  $\tau$  to normal stress  $\sigma$  during slip. The parameters  $c_1$ ,  $c_2$ ,  $c_3$ ,  $f_1$ ,  $f_2$ , and  $f_3$  are constants;  $t$  is the time of contact in seconds; and  $\delta$  is the slip velocity in centimeters per second. During slip at constant velocity,  $t$  was found to be a function of displacement  $\delta$ , velocity  $\dot{\delta}$ , and initial time of contact,  $t_0$ :

$$t = \frac{d_c}{\dot{\delta}} \left( \frac{\delta}{d_c} t_0 \right)^{\exp[(\delta_0 - \delta)/d_c]} \quad (2)$$

where  $\delta_0$  is the initial displacement and  $d_c$  is an experimental parameter with values characteristic of the surface roughness.

For the experiments, hydraulic rams apply shear and normal stress to the sliding surface. Those rams have finite stiffness and therefore interact with the blocks during loading and slip. The series of springs shown in Figure 3 represent the rams in the model. The total stiffness of the springs was specified to give a shear stiffness for slip of 40. MPa/cm, which falls within the range of stiffnesses measured for the hydraulic system under various loads. In the model, motion of the rigid boundaries distorts the springs and applies uniform loads to the sides of the block. To simplify the analysis, the left boundary compresses the springs, while the right boundary extends the springs by an equal amount. Hence there is no change in the total normal stress acting across the surface. For these simulations, normal stress is independently prescribed and may vary systematically by position on the surface. Frictional strength is the product of prescribed normal stress and the coefficient of friction. It will be recalled that inhomogeneity of shear stress relative to strength controls preseismic slip in the experiments. Hence specified variations of normal stress simulate the inhomogeneity that controls preseismic slip.

Quasi-static slip and deformation of the block and loading

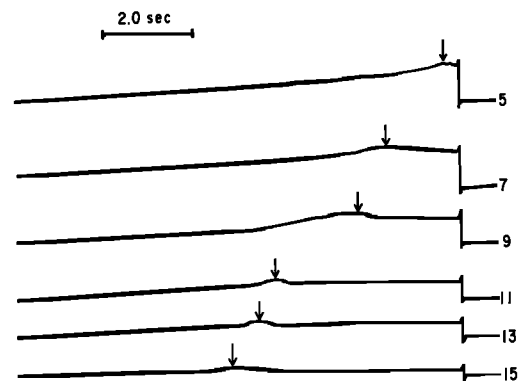


Fig. 2. Shear strain versus time record from Dieterich [1978a]. Numbers refer to the strain gages shown in Figure 1. Arrows mark the beginning of slip at each gage.

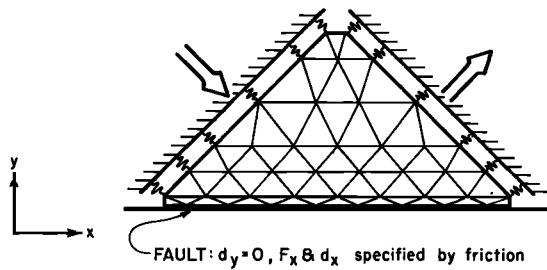


Fig. 3. Finite element model of the experiment shown in Figure 1. Arrows indicate the direction of motion of the rigid boundaries that distort the springs and load the block.

system are computed with the finite element method. The triangular finite element mesh shown in Figure 3 represents the block. The mesh consists of an array of linearly elastic triangular elements connected at nodal points. The Lamé elastic constants are equal to  $2.5 \times 10^4$  MPa. Strains within each element are constant, giving a displacement field that varies linearly by position within the element. Each spring is represented by simple one-dimensional elastic elements with two nodal points that connect the element to the block and to the rigid driving boundary.

Nodal displacements are determined from a system of equations having the form

$$\{F\} = [K]\{\delta\} \quad (3)$$

where  $\{F\}$  is a vector listing the  $x$  and  $y$  components of the nodal forces,  $\{\delta\}$  is the corresponding vector of nodal displacements, and  $[K]$  is the stiffness matrix. Procedures for the determination of  $[K]$  are found in the standard references. Stress and displacement boundary conditions are incorporated into (3) by specifying equivalent nodal forces and nodal displacements. This yields a system of simultaneous equations for the unknown nodal displacements.

Frictional stresses on the sliding surface are represented by lumped nodal forces. For the computations reported here, the sliding surface is assumed to be rigid. Hence the  $y$  component of nodal displacement at each node on the surface is fixed at zero. It is noted that nonuniform displacements on an initially planar surface will cause warping and that the appropriate boundary condition is for constant normal stress instead of fixed displacements perpendicular to the surface. Comparison of results using both boundary conditions yielded indistinguishable slip histories. The displacement condition was chosen because iterative solution of (3) was significantly more rapid than for models with the stress boundary condition and therefore permitted more economical and numerically stable simulations.

A time marching procedure is used to find the displacement fields at successive time steps. The duration of the time steps,  $\Delta T$ , is variable and depends on the rate of loading or the rate of slip. Because  $\mu$  changes over the characteristic displacement  $d_c$ ,  $\Delta T$  is selected to give slip at any point that is much less than  $d_c$ . For the initial stages of slip, when displacement rates are low,

$$\Delta T = (0.1)(\tau)/(K \times R) \quad (4)$$

where  $K$  is the total stiffness of the springs,  $R$  is the rate of displacement of the rigid boundaries that distort the springs, and  $\tau$  is the shear stress. During the later stages of preseismic slip the slip rates accelerate, and the time steps from (4) give displacements that greatly exceed  $d_c$ . Therefore if the maxi-

mum slip displacement  $\Delta\delta$  during a time step is greater than  $d_c/5$ , then the time step  $\Delta T'$  for the next step is set at

$$\Delta T' = d_c \Delta T / (\Delta\delta \times 5) \quad (5)$$

Motion of the rigid boundary connected to the springs is at constant velocity. For each time step those nodal displacements are appropriately incremented and entered as displacement boundary conditions in (3). Along the sliding surface the  $x$  component of either the nodal force or the nodal displacement is specified. Initially, the simulation begins with all displacements on the surface held fixed. The boundary condition changes, permitting the nodes to slide when the applied force equals the frictional force. Conversely, if the velocity of a sliding node is less than or equal to zero, then the displacement of the node is again held fixed.

An iterative procedure coupled to the solution of (3) gives the frictional force from (1) and (2) that satisfies the displacements and velocities. An initial estimate of displacement and sliding velocity of each surface node for the current time step is first obtained by extrapolation of the velocity from the previous time step. From (2), velocity and displacement give an initial estimate of contact time that is used in (1) to obtain  $\mu$  at the end of the time step. This approximation of  $\mu$  is used to find the frictional force for the boundary conditions for (3). Solution of (3) yields improved estimates of displacement, velocity, and  $t$ , which are used again to obtain a better estimate of  $\mu$ . The procedure continues until the solution no longer changes. The simulation is then continued for another time increment. Because the computations are quasi-static, the analysis terminates when unstable slip begins. The criterion for instability in these simulations was for slip velocity in excess of 10 cm/s.

## RESULTS

For these simulations the shear stress on the surface prior to slip varies somewhat with position, especially near the ends. Apparently, the truncated corners of the triangular blocks prevent homogeneous loading by the springs. Because inhomogeneity of shear stress on the sliding surface relative to the frictional strength was found to be a principal determinant of the amount and duration of preseismic slip in experiments, several simulations with different friction distributions relative to initial shear stress were studied. Figure 4 gives the results of a simulation in which the prescribed normal stress distribution was set to give a friction distribution that is everywhere identical to the shear stress. In this case each point on the fault has

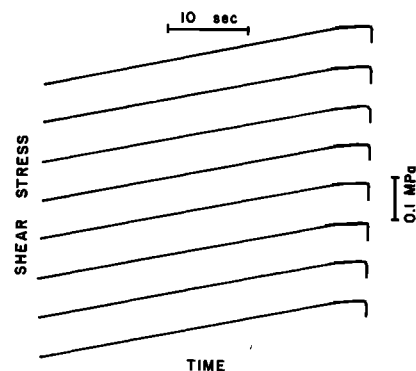


Fig. 4. Computed stress versus time for elements adjacent to the sliding surface. Shear stress prior to slip is homogeneous with respect to the frictional strength.

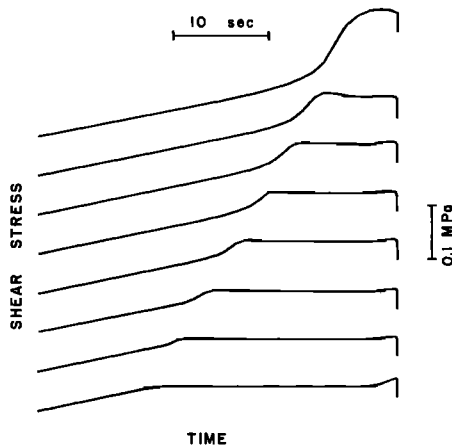


Fig. 5. Computed stress versus time for elements adjacent to the sliding surface showing unilateral propagation of stable slip prior to instability. The difference between frictional strength and shear stress prior to slip increases linearly along the surface.

identical stress and displacement histories. Therefore the simulation corresponds in a general way to the conditions assumed for the spring and slider instability model discussed in the companion paper. However, unlike the spring and slider model the simulation is deterministic and employs the complete constitutive relationships (1) and (2). As a result the events leading to instability can be followed in detail, giving the variation of friction with time, displacement, and velocity. The average shear stress at the beginning of slip is 6.0 MPa. Parameters for  $\mu$  (equation (1)) were based on the results of the companion paper [Dieterich, 1979] and have the following values:  $c_1 = 0.69$ ,  $c_2 = 0.015$ ,  $c_3 = 0.5$ ,  $f_1 = 1.0$ ,  $f_2 = 20.$ , and  $f_3 = 5 \times 10^{-4}$ . Initial time of contact is  $t_0 = 10^4$  s, and  $d_c = 5 \times 10^{-4}$  cm, which is appropriate for the measured center-line-average surface roughness of  $2 \times 10^{-5}$  cm. The boundaries connected to the springs displace at  $10^{-3}$  cm/s.

Figure 4 plots the component of shear stress parallel to the surface as a function of time for the row of elements in Figure 3 that have a single node on the sliding surface. The position of

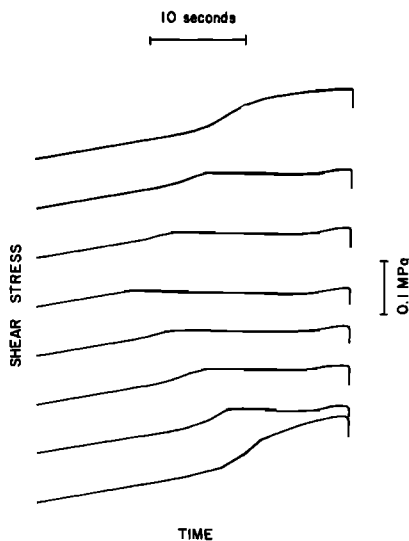


Fig. 6. Computed shear stress versus time for elements adjacent to the sliding surface showing bilateral propagation of stable slip prior to instability.

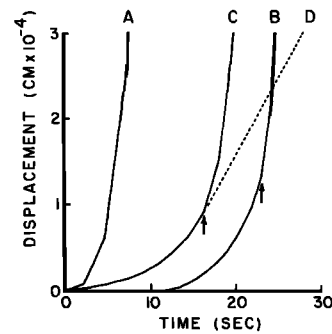


Fig. 7. Displacement versus time for the center nodes in the simulations of Figures 4, 5, 6 (Curves A, B, and C, respectively). The arrows mark the breakout of slip at the end of the sliding surface.

those elements corresponds approximately to the position of the strain gages used in the experiment. As with the experimental results, each curve in Figure 4 is arranged by position on the sliding surface. A leveling or decrease in amplitude of the curves indicates slip adjacent to the element. Although fault slip begins  $\sim 5$  s prior to instability, no significant preseismic slip is evident from the computed strain history of this simulation, because stresses on the fault continue to rise as the slip rates rapidly accelerate. This increase in stress is transient and arises from the velocity term of (1). As shown by Figure 4, slip rapidly accelerates, giving an instability without a propagating preseismic slip event.

Figure 5 gives the stress history for a simulation with a friction distribution similar to that of the experiment shown in Figure 2. For this model the difference between the frictional strength and shear stress prior to slip was specified to increase linearly along the sliding surface. The frictional strengths of the extreme ends of the surface differ by a factor of 1.5. Otherwise, all conditions and parameters for  $\mu$  are identical to the previous simulation. In this case a distinct period of stable sliding of longer duration than that of Figure 4 precedes the slip instability. The results of this simulation resemble the details seen in the experimental result of Figure 2. Slip begins at the end of the surface (bottom curve), where the strength is least and propagates uniformly across the surface. The upturn of the curves immediately prior to slip is caused by slip on the nearby segment of the surface, which increases the rate of loading on the adjacent unslipped portion of the surface. Initially, slip velocities are low, and once slip begins at a node, slip continues with slightly decreasing stress. Instability and rapid stress drop occur only after the propagating front of the boundary between the unslipped and the stably slipping segments of the surface breaks out at the end of the sample. Following breakout the stress and displacements closely resemble those for the initially homogeneous simulation of Figure 4.

Figure 6 gives the results for the model with frictional strength arranged to give a bilateral propagation of preseismic slip. Again the parameters for  $\mu$ ,  $d_c$ , and  $t_0$  are identical to the previous models. In this case the weakest point on the fault is near the middle of the surface, and strength (measured relative to the shear stress) increases linearly toward each end. A sequence of events similar to that of Figure 5 is also seen here. The length of the zone of preseismic slip grows approximately linearly with time, and instability occurs after stable slip has propagated across the entire surface.

The experimental results of Scholz *et al.* [1972] show that

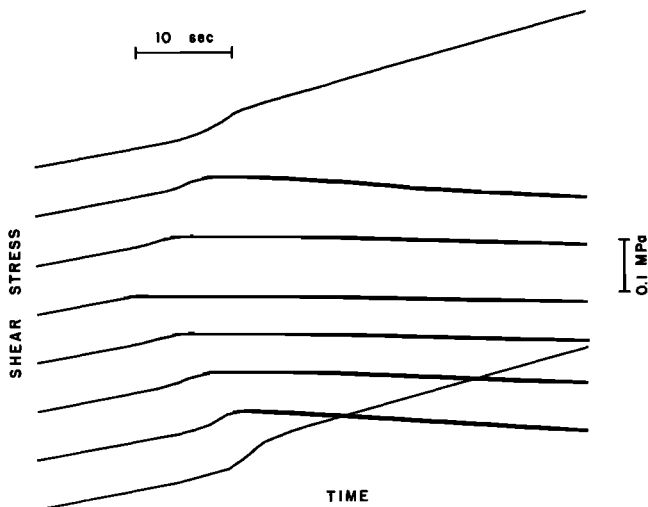


Fig. 8. Computed shear stress versus time for the elements adjacent to the sliding surface. This simulation is identical to the simulation of Figure 6 except the ends of the sliding surface are pinned. Only the first third of the simulation is shown.

preseismic slip rates are initially very low and smoothly accelerate prior to instability. Slip displacements were not recorded in the experiments of *Dieterich* [1978a]. However, *Dieterich* [1978a] presents an analysis that predicts accelerating slip rates assuming a uniform rate of expansion of the area of preseismic slip, constant stress on the slipping segment of the surface, and a constant rate increase of the stress applied to the boundaries of the sample. Figure 7 plots preseismic displacements for a point near the center of the surface against time for the simulations of Figures 4, 5, and 6. The preseismic displacements for the simulation with homogeneous friction relative to initial stress (curve A in Figure 7) are of short duration and rapidly accelerate to instability. In contrast, the displacement curves for nonuniform friction (curves B and C in Figure 7) show a longer period of slowly accelerating slip rates followed by a short period of rapidly accelerating slip. The agreement of the simulations with inhomogeneous friction (Figures 5, 6, and 7) with the strain and displacement records of *Dieterich* [1978a] and *Scholz et al.* [1972], respectively, indicate that the simulations give a good approximation to the phenomena of those experiments. Although slip rates in the simulations accelerate with time, it is interesting to note that the rates of slip at the time of breakout of the slip events are over an order of magnitude less than the rate of loading. Because the entire surface is sliding at that time, the block must then rapidly accelerate to the loading velocity. This jump in slip rates triggers the instability by causing a drop in friction that arises because of the decrease in contact time with velocity given by (2). Additionally, note that the period of rapid slip following breakout and preceding instability is not especially evident in the stress/time plots of Figures 5 and 6 and was probably not measurable from the similar strain/time observations of *Dieterich* [1978a]. Conversely, experimental displacement measurements made some distance from the sliding surface or between loading platens probably show little of the initial slowly accelerating slip that occurs as the area of slip propagates across the surface.

The correlation between triggering of unstable slip and breakout of preseismic slip at the end of the surface was tested with the simulation shown in Figure 8. The conditions for this model are identical to the model of Figure 6 except that the

ends of the sliding surface are pinned. Therefore the zone of preseismic slip was not allowed to break out at the ends of the sliding surface, and slip could not homogenize the stresses to the frictional strength. No instability occurred in this simulation. Unlike the simulations of Figures 5 and 6, slip rates for this model ceased to accelerate when the slip boundary encountered the pinned ends (curve D in Figure 7).

Surface roughness is a principal experimental determinate of slip instability, with smoother surfaces having a greater tendency for unstable slip than do rough surfaces [*Dieterich*, 1978b]. *Dieterich* [1978b, 1979] gives a quantitative explanation for this effect based on the correlation between surface roughness and critical displacement  $d_c$ . The simulation of Figure 9 has conditions identical to those of Figure 6 except that  $d_c = 5.0 \times 10^{-3}$  cm in comparison to  $5 \times 10^{-4}$  cm for the previous simulations. While rapid slip and stress drop occur following breakout of the zone of stable slip, no instability occurs in this simulation. The maximum slip velocity is  $6.4 \times 10^{-2}$  cm/s. Another simulation with  $d_c = 5.0 \times 10^{-2}$  cm greatly smoothed out the accelerated slip event seen in Figure 9 and yielded a maximum slip rate of  $2.5 \times 10^{-3}$  cm/s. The rate of loading in these is equivalent to a slip rate of  $7.1 \times 10^{-4}$  cm/s.

#### DISCUSSION

Some of the general characteristics of preseismic slip have been explored with the above simulations. Overall, the results agree with the phenomena reported by *Dieterich* [1978a] and also appear to be compatible with the data of *Scholz et al.* [1972]. It is concluded that constitutive relationships (1) and (2), which are developed in the companion paper [*Dieterich*, 1979], give an adequate representation of the coefficient of friction as a function of time, displacement, velocity, and surface roughness. It appears that precise simulations of experimental observations can be obtained by careful selection of the model and friction parameters.

Inhomogeneity of stress relative to friction strength controls the initial stages of preseismic slip. For inhomogeneous distributions, in experiments [*Dieterich*, 1978a] and in these simulations, stable slip begins at a point and propagates along the surface. The observations by *Scholz et al.* [1972] that the duration of preseismic slip is inversely proportional to the

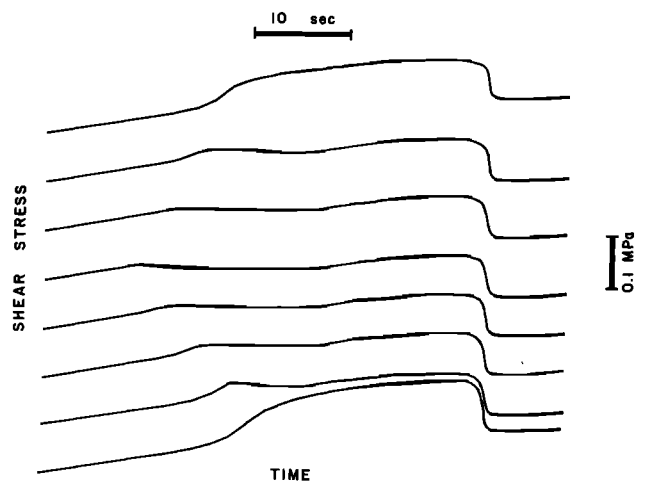


Fig. 9. Computed shear stress versus time for elements adjacent to the sliding surface. The conditions for this simulation are identical to those in Figure 6 except  $d_c = 5 \times 10^{-3}$  cm instead of  $5 \times 10^{-4}$  cm.

loading rate, while the amount of slip and the form of the displacement versus time curves are independent of loading rate, indicate that preseismic slip is controlled by external loading. An analysis by *Dieterich* [1978a] that seems to be confirmed by these simulations suggests that the preseismic displacements observed by *Scholz et al.* [1972] are associated with the growth of the area of preseismic slip. If the surface stress is inhomogeneous with respect to the strength, it is clear that an incremental increase of external loading is required to expand the area of slip incrementally into regions on the surface where the stress is less than the friction. Hence the initial stage of preseismic slip prior to breakout is intrinsically stable and is driven by external loading. This conclusion is supported by the simulation of Figure 8, in which slip breakout at the ends of the sample was not permitted and only stable slip occurred without a rapid stress drop.

Slip instability in the simulations and experiments occurs after preseismic slip breaks out at the ends of the sample. Prior to the breakout, slip rates are less than rates of boundary loading. Hence at the time that slip reaches the end of the surface, slip rates must rapidly increase to the loading rate. However, (1) and (2) predict that friction must decrease with displacement at the higher slip velocities because the time of contact decreases with increasing velocity. The displacement weakening leads to unstable slip.

For application to earthquakes on preexisting faults these results suggest that the earthquake instability may be expected to initiate at the point of a local velocity perturbation during premonitory fault slip. Three mechanisms appear to be possible for causing that perturbation. First, the perturbation could originate as it does in the laboratory if the propagating stage I slip encounters the free surface. Second, experimental results [*Dieterich, 1978a; Dieterich et al., 1978*] indicate that slip velocity will increase in response to an increase in the stage I propagation velocity. That could occur if the slip zone penetrates a more homogeneous zone along the fault. Third, slip velocity must increase if two previously independent zones of stage I slip approach and coalesce to form a single zone. For example, consider two slip zones of equal dimensions  $L$  that are about to merge, and assume that stress on the slipping portions remains constant. Because stress on a dislocation is controlled by the ratio of fault displacement to fault length  $\delta/L$ , the rate of slip must accelerate to double the displacement as the segments merge to form a single zone of length  $2L$ .

Conditions necessary for the occurrence of unstable slip have been outlined by *Dieterich* [1978b] and discussed in the companion paper, using a simple block and spring model and somewhat more primitive constitutive relationships than those employed here. The simple model would appear to approximate the conditions in the experiments only after slip breakout when the stress and friction are homogeneous and the entire block is uniformly sliding. According to the theory, instability occurs if

$$K < \Delta\mu\sigma/d_c \quad (4)$$

where  $K$  is the shear stiffness of the sample and loading system,  $\sigma$  is the normal stress, and  $\Delta\mu$  is the change in the coefficient of friction that takes place over the characteristic displacement  $d_c$ . As originally employed,  $\Delta\mu$  is the difference between friction using the time of static contact and the steady state friction at the loading velocity. However, the results discussed in this study suggest that time of static contact might be altered by preseismic slip. Therefore it would be more appropriate to use contact time when slip breaks out at the end of the sample rather than time of static contact prior to slip.

This raises an interesting point. Considering the uncertainty in the specification of contact time, the analysis of *Dieterich* [1978b] using static time of contact is in surprisingly good agreement with experimental data for the transition from stable to unstable slip as a function of normal stress, stiffness, and surface roughness. For those experiments it is considered likely that preseismic slip took place prior to instability. In the preseismic slip experiments, considerable trial and error were required to give a few events with homogeneous stresses and no preseismic slip. No such care was exercised for the experiments used to analyze the transition from stable to unstable slip. It appears that the analysis of *Dieterich* [1978b] was successful because preseismic displacements were small in comparison to  $d_c$  and at a low velocity. If this were the case, the static time of contact would not be much different than the time of contact, when slip reached the end of the sample. This interpretation is supported by the model simulations of this study. For example, in the simulations of Figures 5 and 6 the initial time of static contact was 10 s, while the average computed times of contact at slip breakout were  $3 \times 10^8$  and  $5 \times 10^9$  s, respectively. By comparison, the time of contact for steady slip at the loading velocity was 0.7 s. Using static time and steady state time with loading velocity in (1) gives  $\Delta\mu = 0.055$ , while use of contact times at slip breakout and steady state contact time gives  $\Delta\mu = 0.046 - 0.050$ . The difference between these values is well within experimental error. Because preseismic displacements apparently increase with the length of the slipping zone, larger sliding surfaces would have proportionally larger preseismic displacements. As a result of the larger displacements, the contact times at the breakout of slip would be significantly reduced (equation (2)), and the use of static contact time would lead to significant error for the prediction of the transition from stable sliding to stick slip.

A principal reason for this detailed study of preseismic slip is the potential relevance to earthquake prediction [*Dieterich, 1978a*]. The consistency with which preseismic slip is observed in laboratory experiments suggests by analogy that preseismic fault displacements may be a regular premonitor to earthquake instability. A source of uncertainty in applying experimental results to earthquake faulting is the question of scaling. Preliminary experiments on a large biaxial sample [*Dieterich et al., 1978*] indicate that preseismic displacements during the initial propagation of slip across the surface scale by fault dimensions and inhomogeneity. The shorter period of rapidly accelerating slip that leads to instability in the simulations is obviously a function of the constitutive relationships, loading rates, and stiffness of the system. Further study of these problems is planned. Of particular importance is the possibility that for earthquake faults, preseismic slip may take place over relatively small fault dimensions, with earthquake slip propagating well beyond the zone of initial slip [*Dieterich, 1978a*]. If this is the general case, then preseismic slip might be of little practical interest for earthquake prediction. Unfortunately, this question may not be accessible by direct experimentation. The good agreement between the results of this study and experimental data suggests that simulations might yield reliable results for earth faulting.

#### REFERENCES

- Byerlee, J. D., and R. Summers, Stable sliding preceding stick-slip on fault surfaces in granite at high pressure, *Pure Appl. Geophys.*, 113, 63-68, 1975.  
 Dieterich, J. H., Preseismic fault slip and earthquake prediction, *J. Geophys. Res.*, 83, 3940-3947, 1978a.

- Dieterich, J. H., Time-dependent friction and the mechanics of stick-slip, *Pure Appl. Geophys.*, 116, 790-806, 1978b.
- Dieterich, J. H., Modeling of rock friction, 1, Experimental results and constitutive equations, *J. Geophys. Res.*, 84, this issue, 1979.
- Dieterich, J. H., D. W. Barber, G. Conrad, and Q. A. Gorton, Pre-seismic slip in a large-scale friction experiment, *Proc. U.S. Rock Mech. Symp. 19th*, 110-117, 1978.
- Logan, J. M., T. Iwasaki, M. Friedman, and S. Kling, Experimental investigation of sliding friction in multilithologic specimens, *Eng. Geol. Case Hist.* 9, 55-67, 1972.
- Scholz, C. H., P. Molnar, and T. Johnson, Detailed studies of frictional sliding of granite and implications for the earthquake mechanism, *J. Geophys. Res.*, 77, 6392-6406, 1972.

(Received April 18, 1978;  
revised December 31, 1978;  
accepted January 10, 1979.)